Applications of AdS/CFT to strongly correlated matter: from numerics to experiments

Chagnet, N.

Chapter 5

Emerging Fermi liquids from regulated quantum electron stars

Attribution

This chapter was published as a journal article under the title "Emerging Fermi liquids from regulated quantum electron stars" in the Journal of High Energy Physics (JHEP), volume 2022, article number 222, together with Vladan Djukić, Mihailo Čubrović and Koenraad Schalm.

5.1 Introduction

Strongly correlated electrons at finite density remain a deep and interesting puzzle, encountered in various quantum-many body systems, from condensed matter to heavy ion physics to astrophysics. Apart from some special cases, Fermi liquids are the only interacting fermionic systems at finite density where we have good control. A breakthrough was provided by the application of AdS/CFT to finite density large N-matrix fermionic systems. This allowed new strongly coupled IR fixed points characterized by an emergent Lifshitz scaling with dynamical critical exponent z to be discovered.[1] Though many of such results were found in bottom-up holographic models where only bosonic operators are tracked, there is reason to believe that any holographic finite density systems must also have microscopic fermionic degrees of freedom. Indeed a number of these holographically discovered fixed points have now been independently confirmed as Sachdev-Ye-Kitaev-like large N quantum spin-liquid fermionic ground

[1] At finite N these fixed points may be not be true IR fixed points but intermediate scale attractors in the RG flow.

states, where the additional microscopic description allows valuable extra insights into the workings of these novel states of matter.

In holography these new ground states are qualitatively understood to arise as a deconfined phase of an underlying microscopic theory with the confined phase corresponding to a conventional Fermi liquid; see [213]. A dozen years ago this was a hotly debated topic and it was found that the prototypical deconfined state, characterized by the AdS_2, $z = \infty$ near horizon dynamics of AdS Reissner-Nordstrom (RN) black holes and an associated multitude N of non-Fermi-liquid Fermi surfaces [214, 215, 32] in the Thomas-Fermi limit of $N \to \infty$ indeed transitions at low temperatures to a charged Tolman-Oppenheimer-Volkov electron star [42, 216, 43, 44, 48]. These states are partially confined - partially deconfined in that they still have a finite z Lifshitz horizon; for a review and the transport responses of these states, see [19, 1].

However, away from the Thomas-Fermi limit a holographic description of a direct single Fermi-surface deconfined non-Fermi-liquid-to-confined Fermi-liquid $T = 0$ quantum phase transition has so far not yet been found. In the bulk, this problem corresponds to solving an Einstein-Maxwell-Dirac system in a self-consistent way, accounting for the backreaction of fermions on geometry, but keeping the number of Fermi surfaces finite or specifically keeping only one. The distinct puzzle here is that the signal of the putative instability towards confinement at low temperature — a log-oscillatory response in the single fermion spectral function [32] — occurs at a distinct point in parameter space from the one where the first stable Fermi surface is located (Fig. 5.1). In [46] an electron star model is introduced where N is finite but still very large; this hinted at a first order rather than a continuous transition. Approaching the question from the other side, a holographic description of confined single Fermi surface Fermi-liquid was constructed in [47] by enforcing confinement through a hard wall IR cut-off [47]. This confirmed that confinement-deconfinement is the correct viewpoint of the quantum phase transition, but did not yet include the gravitational backreaction. The most comprehensive study to date is the attempt at quantum electron star model of [49, 50] which regulates the system by putting it on a sphere and then tries to carefully remove this regularization procedure for a self-consistent solution of the Einstein-Maxwell-Dirac equations in the asymptotic AdS background.

The simple hard-wall solution of [47] already illustrates the fundamental problem. In the presence of an occupied Fermi surface the gravitational backreaction is uncontrolled, see [49, 50]. These subsequent papers then address this by a second cut-off for the backreaction, and then attempt to remove both cut-offs in a precarious balancing act. In the present paper we address this in a different way. We construct a fully gravitationally backreacted single-Fermi surface solution confined through a soft rather than a hard wall. From the gravitational point of view this soft wall determines the deep interior boundary conditions of the fermionic wave functions instead of the horizon geometry. As illustrated in detail in [49, 50] at the technical level the puzzle is that with the vanishing of the horizon (signalling deconfinement) at the quantum

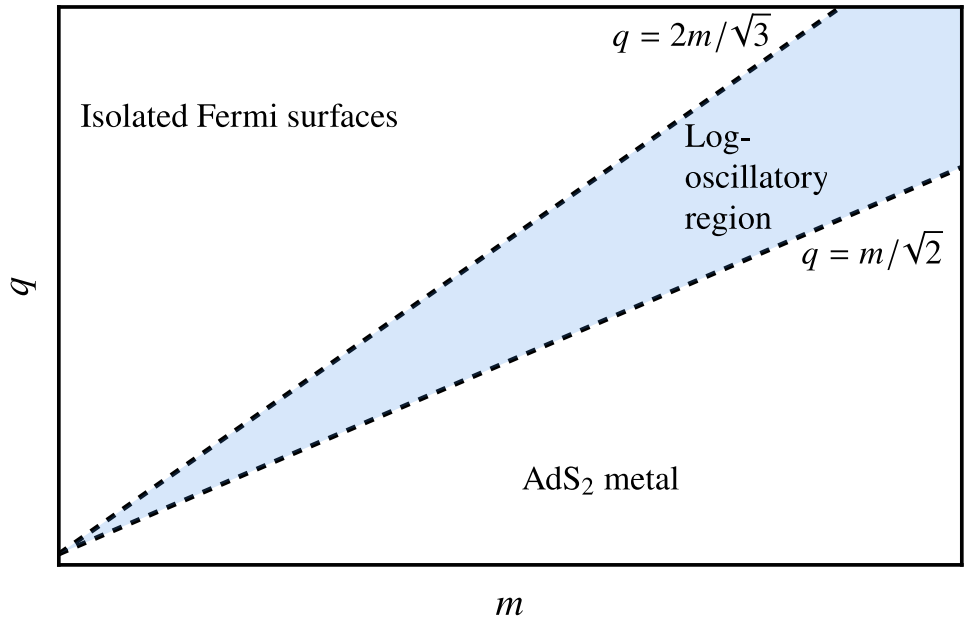

Figure 5.1: A schematic representation of the phase diagram of holographic fermions, where q and m are the charge and the mass (related to the scaling dimension in field theory $\Delta = 3/2 + m$) of the bulk fermion respectively. Along the line $q = m/\sqrt{2}$, determined by the Schwinger pair production threshold, the quantum phase transition ought to happen between the Reissner-Nordström black hole describing the strange metal phase and the quantum electron star solution (no black hole) corresponding to a metallic phase. However, this line is not identical to boundary of the regime where the Reissner-Nordström system supports stable Fermi surfaces as probed through the Reissner-Nordström spectral functions. The electron star (fluid) model requires taking the limit $q, m \to 0$ where both critical lines become indistinguishable. To understand the transition at finite q, m is the motivation for our approach. Adapted from [32].

phase transition, not only must one find a new self-consistent (confining) IR geometry, but also an associated set of self-consistent boundary conditions for the fermion wave-function.

Because the confining boundary conditions suppress the fermion wave function in the IR, there is also no associated backreaction in the deep IR, which remains AdS. This confined regulated quantum electron star (rQES) is therefore the fermionic analogue of the Horowitz-Roberts-Gubser-Rocha AdS_4-to-AdS_4 groundstate/domain wall for holographic superconductors [217, 218]. This solution (just like our soft wall confining electron star solution) describes a system that flows from a conformal pure AdS UV to an intermediate ordered holographic superconductor (Fermi liquid) state with a gap in the sense that below that gap it returns to the renormalized conformal

theory and low energy excitations cannot disturb the ordered state. As is well-known the generic holographic superconductor ground state is not AdS_4-to-AdS_4 but of the Lifshitz type [41]. It is the technical difficulties described above that guided us to first construct this Horowitz-Roberts-Gubser-Rocha type solution. We leave the full Lifshitz quantum electron star for future work. One natural way to construct the latter is that, rather than trying to remove the soft-wall regulator, one can also make it dynamical, similar to the electron star study in [45].

We do confirm that within the class of non-dynamical soft-wall solutions this gapped confined holographic Fermi liquid is the thermodynamically preferred state over the deconfined Reissner-Nordström metallic state for appropriate charge and mass of the fermion. Because we are not yet able to remove the regulator we do not yet solve the puzzle of Fig. 5.1 directly.

The outline of the paper is the following. In Sec. 5.2 we present the gravity setup and the regulated quantum electron star (rQES) solution. In Sec. 5.3, we present the properties of our rQES solution, *i.e.*, the gapped confined Fermi liquid: we show it is the thermodynamically preferred solution in a certain range of parameters, and demonstrate the existence of the infinitely long-lived quasiparticle peaks in the spectrum of the boundary theory. In Sec. 5.4, we present some considerations about removing the confining soft wall. Sec. 5.5 sums up the conclusions together with some musings on further directions of work and the physical meaning of our results.

5.2 A confined Quantum Electron Star: set-up

The minimal bottom-up gravity dual of a strongly correlated electron system is the Einstein-Maxwell-Dirac system [214, 215, 32]. The new element of our setup is the phenomenological soft-wall-like regulator inspired by bottom-up AdS/QCD [219]. The regulator is a fixed non-dynamic scalar field, which neither backreacts on the metric itself nor does it feel the backreaction by the fermions. This is again in line with AdS/QCD models. Therefore, the geometry starts as pure AdS in the UV, in the interior it is influenced by the gauge and matter fields and deviates from AdS, and in far IR all matter fields are exponentially damped by the confining potential. However, in contrast to most hard/soft-wall models we will let the potential only damp the matter sector and not the gravitational sector. The action of the system is:

$$S = \int \mathrm{d}^4x\sqrt{-g}\left[\frac{L^2}{2\kappa^2}\left(R+6\right) - \frac{L^2}{4}F_{\mu\nu}F^{\mu\nu} + L^3\mathcal{L}_f[\Psi,\Phi]\right] \tag{5.1}$$

where κ is the gravitational coupling constant; and L is set to $L=1$ in the remainder. The Dirac Lagrangian is:

$$\mathcal{L}_f = \bar{\Psi}\left[e_A^\mu\Gamma^A\left(\partial_\mu + \frac{1}{4}\omega_\mu^{BC}\Gamma_{BC} - iqA_\mu\right) - \left(m + \hat{M}\Phi\right)\right]\Psi \tag{5.2}$$

where $\bar{\Psi} = i\Psi^\dagger\Gamma^0$, e^μ_A is the vierbein, Γ^A are the gamma matrices in four dimensions, and ω^{AB}_μ is the spin connection. The regulator is fully encoded in an effective mass contribution $\hat{M}(z)\Phi(z)$ for the Dirac field, with $\Phi(z)$ a non-dynamical scalar field whose profile we shall choose later. Inspired by [220], we will consider two types of the confining potential:

$$\hat{M} = \begin{cases} -e^z_3\Gamma^3 \,, & \text{the potential preserves chirality} \,, \\ z\mathbb{1}_4 \,, & \text{the potential breaks chirality} \,. \end{cases} \tag{5.3}$$

Here z, both as index and a variable, refers to the radial coordinate of the AdS space. We will assume a radially symmetric metric which is asymptotically AdS_{d+1} with $d = 3$, parametrized as:

$$\mathrm{d}s^2 = -\frac{f(z)h(z)}{z^2}\mathrm{d}t^2 + \frac{\mathrm{d}x_i\mathrm{d}x^i}{z^2} + \frac{\mathrm{d}z^2}{z^2 f(z)} \,. \tag{5.4}$$

The radial coordinate is defined for $z \geq 0$, where $z = 0$ is the location of AdS boundary (UV). Development of a horizon at finite z is in principle signified by the appearance of a zero of the function f: $f(z_H) = 0$. At zero temperature (the only case we consider), the space extends to infinity, $0 \leq z \leq \infty$.

Our choice to let the wall only confine the fermion-matter sector (together with the absence of backreaction by the confining scalar) implies that at finite chemical potential but zero bulk fermion density, the thermodynamically preferred solution is the regular charged (RN) black hole, though pure AdS with a constant electrostatic potential is also a solution.

For a certain value of the charge q of the fermion, it will be thermodynamically preferred to store all charge in an occupied bulk fermionic state, *i.e.*, nonzero bulk density $n_c \equiv \langle\Psi^\dagger\Psi\rangle$, rather than a Reissner-Nordström black hole. Now the precise radial profile of the scalar $\Phi(z)$ becomes important. The original AdS/QCD papers used a quadratic scalar, behaving in the IR as $\Phi \sim z^2$ [221], which ensures confinement while still being smooth. Another form found in the literature is a profile which flattens out to a constant in the IR [222]. At the same time the UV completion of the scalar field has to ensure that its contribution to the Dirac equation decays quickly enough for small z to reproduce the equation of motion in pure AdS in the limit $z \to 0$. The forms that satisfy all the requirements and which we find numerically convenient are

$$\begin{aligned} &\Phi(z) = \lambda z^2, && \text{quadratic scalar} \\ &\Phi(z) = \lambda\frac{z^\alpha}{z_0^\alpha + z^\alpha}, && \text{flat scalar.} \end{aligned} \tag{5.5}$$

The amplitude of the scalar (*i.e.*, the measure of the "hardness" of the wall) is parametrized by λ, and z_0 is the scale at which the scalar begins to flatten (in the second, flat scalar model). The choice of α is merely that of computational convenience and we choose $\alpha = 4$. Similarly, we will consistently choose $z_0 = 2$ throughout the rest of this paper.

5.2.1 Einstein-Maxwell-Dirac equations

From the action we obtain the Maxwell equation and two convenient linear combinations of the tt and zz components of the Einstein equations. With the ansatz that only $A_t \neq 0$, and that all functions only depend on z, compatible with homogeneity and isotropy, they reduce to

$$\begin{aligned} A_t''(z) - \frac{h'(z)}{2h(z)} A_t'(z) &= \sqrt{h(z)} n(z) \,, \\ 1 + \frac{z}{3} f'(z) - f(z) &= \frac{z^2}{3 f(z) h(z)} \rho(z) + \frac{z^4}{12 h(z)} A_t'(z)^2 \,, \\ h'(z) &= -z h(z) p(z) - \frac{z}{f(z)^2} \rho(z) \,. \end{aligned} \tag{5.6}$$

Compatible with the symmetries the current vanishes $J^i = 0$, the charge density J^0 is denoted as $J^0 = n(z)/\sqrt{-g} = z^4 n(z)/\sqrt{h(z)}$, and the stress tensor is parametrized as

$$(T_f)_{\mu\nu} = \mathrm{diag}(\rho(z), p_\perp(z), p_\perp(z), p(z)), \tag{5.7}$$

where $p_\perp(z)$ is the pressure in the transverse x, y directions.

The ii components of the Einstein equations are both equal to

$$\begin{aligned} z h(z) \left[-z^3 A_t'(z)^2 + \left(3 z f'(z) - 4 f(z) \right) h'(z) + 2 z f(z) h''(z) \right] + \\ + 2 h(z)^2 \left[z \left(z f''(z) - 4 f'(z) - 2 \beta z p_\perp(z) \right) + 6 f(z) - 6 \right] - z^2 f(z) h'(z)^2 = 0 \,. \end{aligned}$$

They are not independent, however. Denoting the Einstein field equations as $E_{\mu\nu} \equiv G_{\mu\nu} - T_{\mu\nu}$ and the Maxwell equation as $E_M \equiv \nabla_\mu F^{\mu\nu} - J^\nu$, one can show that[2]

$$E_{xx} = \hat{L} \cdot E - \frac{1}{2z} \nabla_\mu T^{\mu\nu} \,, \tag{5.8}$$

where $\hat{L} \cdot E \equiv A_1 \partial_z E_{tt} + A_2 \partial_z E_{zz} + A_3 E_M + A_4 f'(z) E_{tt} + E_{zz} \left(A_5 f'(z) + A_6 h'(z) + A_7 \right)$ is a linear combination of both $\{E_{tt}, E_{zz}, E_M\}$ and their derivatives and $T^{\mu\nu}$ is the total stress-energy tensor associated with the matter content of the theory. The stress-tensor is covariantly conserved if the matter sector is on-shell, *i.e.*, obeys its equations of motion. Thus

$$E_{xx}^{\text{on-shell}} = \nabla_\mu T^{\mu\nu} = 0 \tag{5.9}$$

It is therefore sufficient to solve the three equations (5.6) together with the matter sector.

The charge, energy and pressure densities $n(z), \rho(z), p(z)$ are determined by the occupied fermionic states in the AdS bulk space. Importantly, we will compute them

[2] This is essentially $\nabla_\mu G^{\mu\nu} = \nabla_\mu T^{\mu\nu}$.

solely from microscopic considerations: we do *not* assume anything like a fluid limit or a specific form of the equation of state. We compute them from the Dirac Lagrangian, within the one-loop Hartree correction to the background. This is discussed in detail in the next subsection.

We will now proceed to derive the equation of motion for the Dirac field. From (5.2), the equation reads:

$$e_A^\mu \Gamma^A \left(\partial_\mu + \frac{1}{4}\omega_\mu^{BC}\Gamma_{BC} - iqA_\mu\right)\Psi = \left(m + \hat{M}(z)\Phi\right)\Psi\,. \tag{5.10}$$

It is known that the spin connection in this type of metric can be eliminated by rescaling the fermion [214, 223]:

$$\Psi = \left(-g^{zz}\det g_{\mu\nu}\right)^{-\frac{1}{4}}\tilde{\psi} = \left(\frac{f(z)h(z)}{z^{2d}}\right)^{-\frac{1}{4}}\tilde{\psi} \equiv a(z)\tilde{\psi}. \tag{5.11}$$

In addition, it is convenient to eliminate any singular terms from the fermionic wavefunction. Since our solutions are smooth in the interior as we shall see, the only singularity is the branch cut in the UV behaving as z^m. We thus rescale one more time

$$\tilde{\psi} = z^m\psi \equiv b(z)\psi. \tag{5.12}$$

In most cases we will use the rescaled form and write the equations for ψ. So far this is all independent of the gamma matrix representation. In order to simplify the equations of motion, we now employ the representation

$$\Gamma^\mu = \begin{pmatrix} 0 & \gamma^\mu \\ \gamma^\mu & 0 \end{pmatrix},\ \Gamma^3 = \begin{pmatrix} 1 & 0 \\ 0 & -1 \end{pmatrix}, \tag{5.13}$$

with $\mu \in \{0,1,2\}$, $\gamma^0 = i\sigma^2, \gamma^1 = \sigma^1, \gamma^2 = \sigma^3$ and $\sigma^{1,2,3}$ are the usual Pauli matrices. Homogeneity and isotropy along the t,x,y directions allow us to take the energy ω and momentum $k \equiv k_x$ as good quantum numbers, so the Dirac bispinor is expressed as

$$\psi = e^{-i\omega t + ikx}\left(\psi_1(z), \chi_1(z), -i\chi_2(z), i\psi_2(z)\right)^T. \tag{5.14}$$

As in [47, 223], this yields two (equivalent) decoupled systems for the two independent components, for $\psi_{1,2}$ and $\chi_{1,2}$, corresponding to the spin degeneracy of our system. We will focus on the ψ_i components for which the Dirac equation reads

$$\begin{aligned}
&\left[\partial_z + \varepsilon_+\Phi + \frac{m}{z}\left(1 - \frac{1}{\sqrt{f(z)}}\right)\right]\psi_1(z) - \left[\frac{k}{\sqrt{f(z)}} + \frac{\omega + qA_t}{f(z)\sqrt{h(z)}}\right]\psi_2(z) = 0 \\
&\left[\partial_z + \varepsilon_-\Phi + \frac{m}{z}\left(1 + \frac{1}{\sqrt{f(z)}}\right)\right]\psi_2(z) + \left[\frac{\omega + qA_t}{f(z)\sqrt{h(z)}} - \frac{k}{\sqrt{f(z)}}\right]\psi_1(z) = 0\,.
\end{aligned} \tag{5.15}$$

where $\varepsilon_+ = \varepsilon_- = 1$ corresponds to the chiral-preserving potential and $\varepsilon_+ = -\varepsilon_- = -1/\sqrt{f(z)}$ corresponds to the chiral-breaking potentials.

5.2.2 Fermion densities and backreaction

The fermionic densities and pressures are obtained microscopically, from the Dirac Lagrangian (5.2):

$$\begin{aligned} \rho &= \langle \Psi^\dagger e_0^t \Gamma^0 (-i\omega - iqA_t)\Psi \rangle \,, \\ n &= -\langle \Psi^\dagger \Psi \rangle \,. \end{aligned} \tag{5.16}$$

The components of the pressure $p_\perp, p$ are likewise formally equal to

$$\begin{aligned} p_\perp &= \langle \bar{\Psi} i e_1^x k_x \Gamma^1 \Psi \rangle, \\ p &= \langle \bar{\Psi} e_3^z \Gamma^3 \partial_z \Psi \rangle. \end{aligned} \tag{5.17}$$

The expectation value $\langle \ldots \rangle$ in (5.16-5.17) is the quantum-mechanical expectation value, *i.e.*, one solves the Dirac equation with appropriate boundary conditions (see below) and sums over the quantum numbers in the appropriate range. The quantum numbers are the radial modes ℓ, and momenta k_x, k_y in the x, y-directions which determine the on-shell energy in terms of a dispersion relation $\omega = E_\ell(k)$. The role of the confining potential is essential here: it quantizes the radial number ℓ. Each discrete radial mode corresponds to a separate Fermi surface [214, 215, 32, 44, 48, 47]. As emphasized in the Introduction, we seek a state where only a single Fermi surface is occupied. This must be the lowest radial mode. Note that despite occupying a single mode, this mode still contains a thermodynamically large number of states counted by the x, y-momenta. Each radial mode is thus a fluid of fermions.

We will ignore the subtleties of the zero-point energy and the Dirac sea; in principle these are absorbed in a renormalization of the cosmological constant and the AdS radius; see however [49, 50] for a more detailed treatment. Then, in terms of the solutions to the Dirac equation, formally the expressions for the density are

$$\begin{aligned} n(z) &= \frac{2q}{z^3\sqrt{f(z)}} a(z)^2 b(z)^2 \sum_{k,\ell} \Theta\left(-E_\ell(k)\right) \left(\psi^\dagger_{1;\ell,k}(z)\psi_{1;\ell,k}(z) + \psi^\dagger_{2;\ell,k}(z)\psi_{2;\ell,k}(z)\right) \\ \rho(z) &= a(z)^2 b(z)^2 e_0^t(z)\left(-i\omega - iqA_t(z)\right) \sum_{k,\ell} \Theta\left(-E_\ell(k)\right) \left(\psi^\dagger_{1;\ell,k}(z)\psi_{1;\ell,k}(z) + \psi^\dagger_{2;\ell,k}(z)\psi_{2;\ell,k}(z)\right) \\ p(z) &= a(z)^2 b(z)^2 e_3^z(z) \sum_{k,\ell} \Theta\left(-E_\ell(k)\right) \left(\psi^\dagger_{1;\ell,k}\partial_z\psi_{2;\ell,k} - \psi^\dagger_{2;\ell,k}\partial_z\psi_{1;\ell,k}\right) \end{aligned} \tag{5.18}$$

where the step-function $\Theta(x)$ selects the positive energy states. Note that due to the antisymmetry of the two spin components, the derivatives of the scaling factors $a(z), b(z)$ cancel out in the expression for p.

The self-consistent Hartree calculation

We solve the system (5.6, 5.15) in the one-loop Hartree approximation. As a reminder, the Hartree correction is the local single-particle diagram (vacuum bubble),

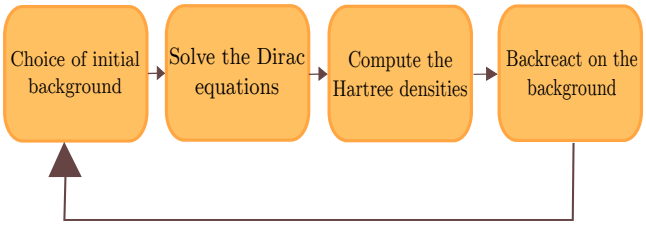

Figure 5.2: Iteration algorithm used to compute the rQES solution.

ignoring anti-particles, *i.e.*, ignoring the contribution from the Dirac sea. We do not take into account the Fock correction. In flat space, the Hartree correction is trivial [224]: in terms of the causal fermionic propagator G_R it equals $\lim_{t\to 0-}\int \mathrm{d}\omega \mathrm{d}^2k\; G_R(\omega,k)e^{-i\omega t} = \delta\mu$,[3] merely renormalizing the chemical potential. In curved space however, the local chemical potential is $\mu_{\rm loc}(z) = A_t(z)\sqrt{-g^{tt}(z)}$, with a nontrivial radial profile, thus the correction $\delta\mu(z)$ is also variable along z and therefore it can have nontrivial physical effects.

The Hartree approximation then proceeds by computing this one-loop Hartree correction self-consistently. One starts with an ansatz for the background, solves the Dirac equation in this background, computes the one-loop Hartree densities in the assumption that they are small, updates the background and iterates to convergence as in Fig. 5.2.

5.2.3 Boundary conditions on the Einstein-Maxwell sector

The Einstein-Maxwell equations (5.6) require four boundary conditions in total (two for $A_t(z)$ and one for each of the metric functions $f(z), h(z)$). The UV boundary conditions are

$$\begin{aligned} A_t(z_{\rm UV}) &= \mu\,, && \text{the chemical potential.} \\ f(z_{\rm UV}) &= h(z_{\rm UV}) = 1\,, && \mathrm{AdS}_4 \text{ asymptotics.} \end{aligned} \tag{5.19}$$

[3] The infinitesimal time separation $t \to 0-$ is really the point-splitting regularization, as the integral of G_R at coincident points in spacetime generally diverges; the sign of t is dictated by the contour choice for the retarded propagator [224].

The fourth boundary condition we impose is given by our demand that we seek a state where *all* the charge is contained in occupied fermionic states.[4] The confining potential ensures that the fermionic wavefunctions are localized at a finite value in the radial direction. Thus by construction the charge density will vanish in the deep AdS interior. From this follows that the fourth boundary condition is $\partial_z A_t(z_{\rm IR}) = 0$. Formally $z_{\rm IR} = \infty$; in our numerical computation it will be finite but large, and we have checked that our results do not depend on its value.

In practice, we solve the boundary value problem by shooting from the IR. We impose directly the condition $\partial_z A_t(z_{\rm IR}) = 0$ as well as the condition $\partial_z f(z_{\rm IR}) = 0$. The latter indirectly encodes our demand that we seek a $T = 0$ solution; recall that for a black hole solution $\partial_z f(z_{\rm horizon}) \sim T$. Then we use the free value $A_t(z_{\rm IR})$ and $h(z_{\rm IR})$ to shoot for $A_t(z_{\rm UV}) = \mu,\ h(z_{\rm UV}) = 1$ at the boundary. From the equation of motion for $f(z)$ one obtains automatically that $f(z_{\rm IR}) = 1$ once we fall on the right branch; for the same reason one can also use $f(z_{\rm IR}) = 1$ as an IR boundary condition if one demands in addition that there is no energy density or electric field in the deep interior.

5.2.4 Boundary conditions for the fermions

The UV boundary conditions for the appropriate solutions to the Dirac equation are straightforward. Near the AdS boundary the rescaled field behaves as

$$\begin{aligned}\psi_1(z\to 0) &\sim A_\ell(\omega,k)\frac{\omega-k-\mu q}{2m-1}z^{1-2m} + B_\ell(\omega,k) + \dots,\\ \psi_2(z\to 0) &\sim A_\ell(\omega,k)\, z^{-2m} + B_\ell(\omega,k)\frac{\omega+k-\mu q}{2m+1}z + \dots\ .\end{aligned} \tag{5.20}$$

On-shell solutions are normalizable, *i.e.*, $A_\ell(\omega,k) = 0$. This agrees with the AdS/CFT dictionary, where a finite $A_\ell(\omega,k)$ would imply an external source for the fermions for a specific band ℓ and energy ω, k. Demanding normalizability $A_\ell(\omega,k) = 0$ instead, implicitly translates in a dispersion relation $\omega(k) = E_\ell(k)$.

The IR boundary conditions for the fermions require a more detailed discussion. Firstly, for the fermionic wavefunctions, the amplitude is set by normalization of each wavefunction to unity. For each radial mode ℓ this implies

$$\int dz\sqrt{-g}|\psi_{i;\ell,k}(z)|^2 < \infty. \tag{5.21}$$

For finite temperature backgrounds this is usually not an issue as the horizon is parametrically at finite distance and finite IR boundary conditions, together with the UV-condition that the un-normalizable fall-off vanish, guarantees a finite integral. For the $T = 0$ background we consider here, the interior is parametrically at infinite

[4] There could be interpolating solutions with both a charged horizon and a charge in occupied fermionic states. We will not seek for those here as the presence of the charged Reissner-Nordstrom like horizons should imply the continued presence of log-oscillatory instabilities.

distance and finiteness of the integral can only follow from bounded behavior of the wavefunction. Since the spin components are not independent, it is sufficient to demand $\psi_{1;\ell}(z \to \infty) \to 0$, *i.e.*, the leading component should vanish in the interior.

It is well known in AdS/CFT that it is then the simultaneous requirement of a UV and an IR boundary condition that determines the spectrum of the small excitations. This spectrum can still be continuous or discrete; we address this directly below. Formally, however, the normalization together with two boundary conditions make the system overconstrained and one must search for accidental solutions. We again do so by shooting from the interior to search for parameters where the UV conditions are also satisfied.

The shooting condition we use is the ratio ψ_2/ψ_1, which still leaves the freedom to normalize the norm (5.21) to unity, and which we do after the solution is found.

Effective potentials and confinement

Pure $T = 0$ AdS — representing a deconfined phase of the strongly coupled boundary theory — has a continuum spectrum of normal modes computed in the way described above. The system must be considered in a different phase or have its IR dynamics modified by a confining potential to discretize the spectrum; this spectrum may still be ungapped or gapped. We will now demonstrate that the chiral-breaking soft-confining potential supports a discrete Fermi surface, *i.e.*, a tower of bound states at discrete energies, for momenta up to some k_F, the Fermi momentum. The spectrum is also gapped. A convenient way to see the effect of this potential is to transform the Dirac equation to the Schrödinger form [32, 48, 19]:

$$\begin{aligned} &\chi_{\text{Sch}}(z) = e^{\frac{1}{2}\int_0^z \mathrm{d}u\, \mathcal{P}(u)}\,, \\ &\left[\partial_z^2 - V(z)\right]\chi_{\text{Sch}}(z) = 0\,, \\ &V(z) = \frac{1}{2}\mathcal{P}'(z) + \frac{1}{4}\mathcal{P}(z)^2 - \mathcal{Q}(z)\,, \end{aligned} \tag{5.22}$$

where the coupled equations (5.15) were decoupled into two second order equations, each taking the form

$$\psi''(z) + \mathcal{P}(z)\psi'(z) + \mathcal{Q}(z)\psi(z) = 0\,, \tag{5.23}$$

with the indices 1,2 on $\psi, \chi_{\text{Sch}}(z), V$ omitted.

In principle, the Schrödinger potential is itself a function of the background spacetime and electrostatic potential $f(z), h(z), A_t(z)$ and can be fully determined only by calculating numerically the full solution. However, we can give a qualitative estimate whether it is confining or not by studying its asymptotics. Since the bulk remains asymptotically AdS_4, we have $V(z \to 0) \sim \frac{1}{z^2}$. In pure AdS_4 the IR behavior

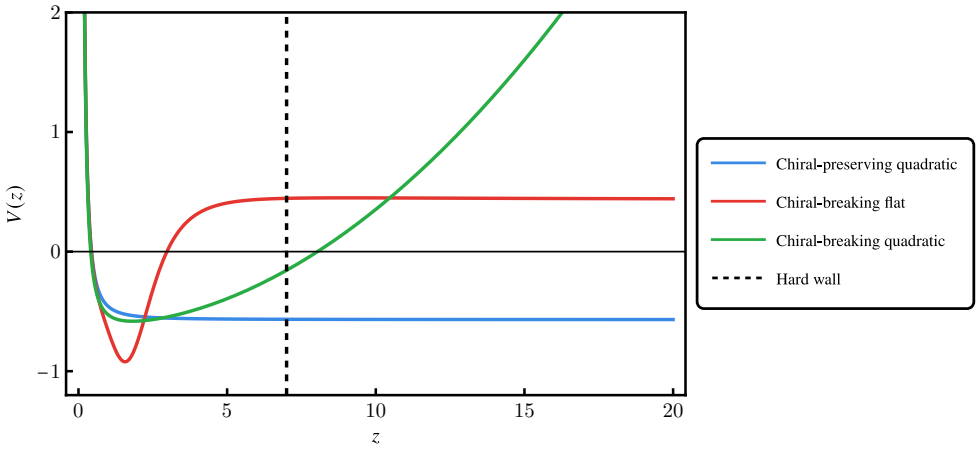

Figure 5.3: Comparison of the Schrödinger potentials for $\psi_1(z)$ for the two types of confining potential: chiral-breaking quadratic (green), chiral-breaking flat (red) and chiral-preserving quadratic (blue). The dashed black line indicates the truncation of spacetime which happens in the hard wall model of [47] at $z = 7$. Only the chiral-breaking potential and the hard wall allow for bound states. Parameters are $\{m, \mu q, k, \omega\} = \{0.1, 1.05, 0, -0.027\}$. The scalar parameters are $\lambda = 0.1$ for the two quadratic scalars and $\lambda = 1$ for the flat scalar.

would be $V_{\text{AdS-IR}}(z \to \infty) = -(\omega + \mu q)^2 + k^2 + m(m+1)/z^2 + \mathcal{O}(1/z^3)$ (Fig. 5.3).[5] This now gets modified by the confining potential due to the scalar $\Phi(z)$. Making the ansatz that the confining potential in the deep IR for $z \to \infty$ suppresses exponentially all sources in the Einstein and Maxwell equations for large z, *i.e.*, the geometry in the deep IR is again an (emergent) AdS_4 geometry, the leading order IR behavior of the potential is then schematically

$$V_{\text{AdS-IR}} = V(z \to \infty) + (\varepsilon_- - \varepsilon_+)\left[-\frac{\phi'(z)}{2z} + \frac{\phi(z)(4m+2) + (\varepsilon_- - \varepsilon_+)\phi(z)^2}{4z^2} + \right] + \mathcal{O}(1/z^3)\,, \tag{5.24}$$

Note that the chiral-preserving solution $\varepsilon_+ = \varepsilon_- = 1$ leads to a vanishing contribution and therefore does not lead to fermionic bound states. In contrast the chiral-breaking solution $\varepsilon_+ = -\varepsilon_- = -1/\sqrt{f(z)} = -1 + \mathcal{O}(1/z)$ in an AdS_4 IR does lead to a potentially bounding potential depending on the choice of $\Phi(z)$. For this reason, we will work solely with the chiral-breaking scalar field.

Fig. 5.3 shows the behavior of the Schrödinger potential for the various profiles of the scalar field and regulation schemes. With a chiral-breaking regulator, we indeed see that the infrared behavior of the potential is dominated by the large z behavior of

[5] We are interested in $k^2 < (\omega + \mu q)^2$ since the potential is otherwise confining even in AdS_4 with no regulator, as discussed in [225]. We will discuss this later.

each profile. The final choice of which scalar field profile to use is determined by the convergence of the iteration scheme. We numerically found the quadratic profile to be unstable while the flat profile leads to an emergent AdS_4 in the infrared. Specifically for the chiral-breaking confining potential with flat asymptotics the Schrödinger potential in the deep IR becomes

$$V(z \to z_{\rm IR}) = -\omega_{\rm IR}^2 + \lambda_{\rm IR}^2 + k_{\rm IR}^2 + \mathcal{O}(1/z) \equiv V_{\rm IR} + \mathcal{O}(1/z), \tag{5.25}$$

where we have used that $f(z), h(z), A_t(z)$ become constant in the emergent AdS_4 IR and we have defined $\omega_{\rm IR} \equiv \dfrac{\omega + qA_t(z_{\rm IR})}{f(z_{\rm IR})\sqrt{h(z_{\rm IR})}}$, $\lambda_{\rm IR} \equiv \dfrac{\lambda}{\sqrt{f(z_{\rm IR})}}$ and $k_{\rm IR} \equiv \dfrac{k}{\sqrt{f(z_{\rm IR})}}$.

In the IR limit, Schrödinger equation becomes

$$\left[\partial_z^2 - V_{\rm IR}\right] \chi_{\rm Sch}(z) = 0\ , \tag{5.26}$$

which is solved by

$$\chi_{\rm Sch}(z) = \chi_{\rm Sch+}(z) e^{\sqrt{V_{\rm IR}} z} + \chi_{\rm Sch-}(z) e^{-\sqrt{V_{\rm IR}} z}\ . \tag{5.27}$$

We see from (5.27) that, for frequencies such that $V_{\rm IR} > 0$, the solutions have a growing and a decaying branch. The decaying branch clearly confines the wavefunction. This is the one we shall choose. This leads to the following IR form for our original Dirac fermion components

$$\psi_{1,2}^{\rm IR}(z) = c_{1,2}^{\rm IR}(z) e^{-\sqrt{V_{\rm IR}} z}\ , \tag{5.28}$$

where the ratio of the coefficients is fixed by the Dirac equation (5.15):

$$\frac{\psi_2^{\rm IR}(z)}{\psi_1^{\rm IR}(z)} = \frac{c_2^{\rm IR}(z)}{c_1^{\rm IR}(z)} = \frac{1}{\omega_{\rm IR} + k_{\rm IR}} \left[\frac{m}{z} \left(\frac{1}{\sqrt{f_{\rm IR}}} - 1 \right) + \sqrt{V_{\rm IR}} + \lambda_{\rm IR} \right] \tag{5.29}$$

and the normalization of the wavefunction to unity sets the remaining overall scale. With these IR boundary conditions the equations (5.15) are solved by shooting from $z_{\rm IR}$ to $z_{\rm UV}$.

The confinement imposed by both IR and UV boundary conditions leads to a discrete and gapped spectrum which defines a band structure (see Fig. 5.6 later). The fall-off of the wavefunction both at the AdS boundary and the interior also implies an absence of any backreaction in those regions. Once backreaction is included the resulting solutions will therefore be AdS_4-to-AdS_4 domain wall solutions, as we will show in the next section.

As a last remark, equation (5.25) gives us a simple way to view the effect of the chiral-breaking flat potential. As has been pointed out in [32, 225], in AdS_4 with constant electrostatic potential where $\lambda = 0$, the potential is deconfining for modes with $|\omega_{\rm IR}| > |k_{\rm IR}|$ and confining for modes such that $|\omega_{\rm IR}| < |k_{\rm IR}|$. The addition of a

flat profile means that now modes with $|k_{\rm IR}| \leq |\omega_{\rm IR}| < \sqrt{k_{\rm IR}^2 + \lambda_{\rm IR}^2}$, which previously were not bound states, also become confined. This allows the existence of a window $\omega_-(k) < \omega < \omega_+(k)$, with $\omega_\pm(k) \equiv qA_t(z_{\rm IR}) \pm \sqrt{k_{\rm IR}^2 + \lambda_{\rm IR}^2}$ where a discrete set of (gapped) modes can be populated.

5.3 Regulated Quantum Electron Star: thermodynamics and spectrum

Now that the problem is well-posed, we can follow the algorithm in Fig. 5.2 and construct a fully backreacted regulator-confined $T = 0$ quantum electron star. Choosing the chirality-breaking flat regulator the resulting solution is shown in Fig. 5.4. This is by construction an AdS_4-to-AdS_4 domain wall solution. Just like the analogous domain wall solutions for the holographic superconductor [218, 41, 217], it has a UV AdS_4 and an IR AdS_4 with the *same* radius but different effective speed of light. This can be checked by considering the diffeomorphism-invariant ratios $v_{\rm IR}/v_{\rm UV}$ and $L_{\rm IR}/L_{\rm UV}$ which are equal to

$$\frac{L_{\rm IR}}{L_{\rm UV}} = \sqrt{\frac{R(z \to z_{\rm UV})}{R(z \to z_{\rm IR})}} = 1 \,, \quad \frac{v_{\rm IR}}{v_{\rm UV}} \equiv \frac{v(z \to z_{\rm IR})}{v(z \to z_{\rm UV})} = \sqrt{\frac{h(z \to z_{\rm IR})}{h(z \to z_{\rm UV})}} < 1 \text{ in our solution} \,. \tag{5.30}$$

Here $R(z)$ is the Ricci scalar and $v(z) = \sqrt{h(z)}$ is deduced from the null vector $\frac{\mathrm{d}}{\mathrm{d}t} X^\mu(z)$ where $X^\mu(z) \equiv \{t, 0, v(z)t, 0\}$ is a x-directed trajectory. Therefore, our solution obeys the c-theorem since the effective speed of light in the dual field theory is lower in the IR than in the UV, as discussed in detail in [218].

In accordance with our discussion in the Introduction, the chemical potential is chosen such that only the lowest radial mode of the fermionic wavefunction is occupied. The associated matter content shows that a localized distribution of fermions in the mid-infrared region is characterized by a stable finite density of fermions with total charge $Q = -A_t'(z \to 0)$.

With the chirality-breaking flat potential the convergence is in fact quite fast at low density. The Hartree algorithm provides a discrete sequence of fields $(f^{(n)}, h^{(n)}, A_t^{(n)})$ as we iterate from $n = 1, 2, \ldots$. We can introduce a criterion for the convergence of the solution using the IR parameters used for shooting

$$\epsilon_n = \sqrt{f^{(n)}(z_{\rm IR})^2 + A_t^{(n)}(z_{\rm IR})^2 + h^{(n)}(z_{\rm IR})^2} \,, \tag{5.31}$$

Convergence is obtained if $(\Delta\epsilon)_n \equiv \epsilon_n - \epsilon_{n-1} \xrightarrow{n\to\infty} 0$. For a small occupation number/charge Fig. 5.5 shows that the solution already stabilizes after three iterations; for large occupation numbers the convergence rapidly becomes much slower. We have checked that the solution is not sensitive to the choice of the numerical cutoffs $\{z_{\rm UV}, z_{\rm IR}\}$.

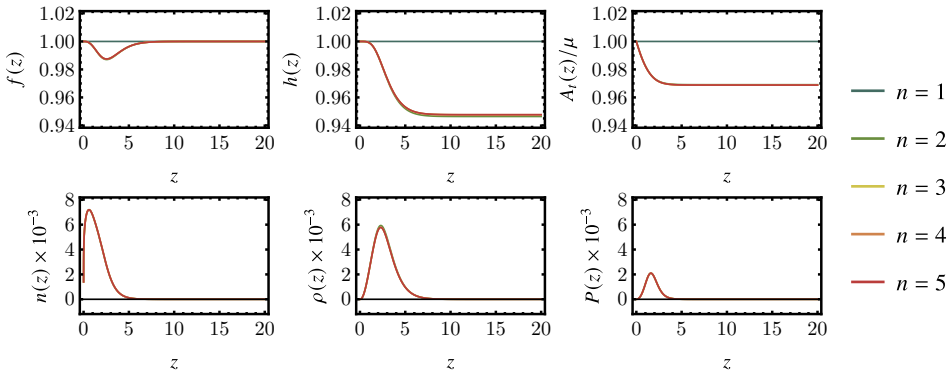

Figure 5.4: Iterative backreactions on the background fields ($f(z)$, $h(z)$,$A_t(z)$) and their associated currents ($n(z),\rho(z),P(z)$) with the same parameters as in Fig. 5.5. In total 5 iterations are performed, denoted by the color scale from violet (first iteration) to red (last iteration). For these values $\{m,\mu q,\lambda\} = \{0.1,0.9,1\}$ only the first iteration differs significantly from the final solution, and the other curves are visually barely distinguishable from each other; for higher q convergence rapidly becomes slower.

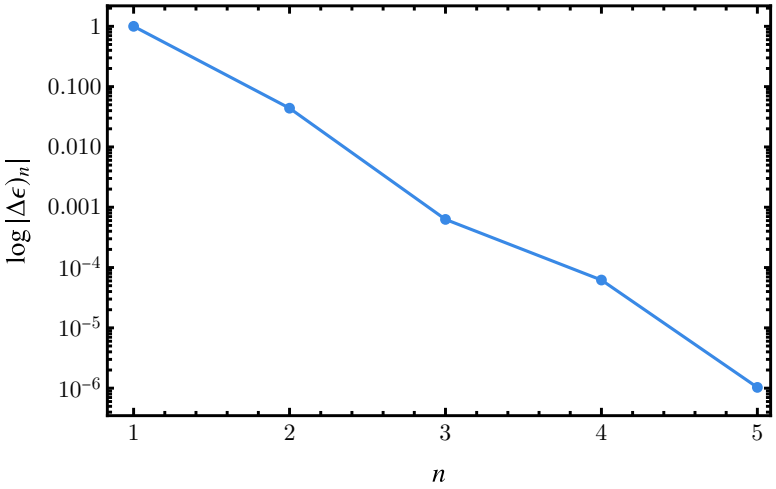

Figure 5.5: Convergence in terms of the logarithm of the difference in the IR between the n-th and $n+1$-st iteration $(\Delta\epsilon)_n$ for a rQES with $\{m,\mu q,\lambda\} = \{0.1,0.9,1\}$. he convergence is exponentially fast and the agreement is very good already around the 3$^{\text{rd}}$ iteration. The convergence is very good already around the 3$^{\text{rd}}$ iteration.

5.3.1 Thermodynamics

For a large q/m ratio we expect that the quantum electron star at a given chemical potential μ is the thermodynamically preferred solution over the extremal Reissner-

Nordström solution. In order to study the thermodynamics of the regulated quantum electron star, we need to compute its free energy. It consists of two parts. There is a direct saddle point contribution from the regularized Euclidean action:

$$S_E = \int \mathrm{d}^4x\sqrt{g_E}\left[\frac{1}{2\kappa^2}\left(R+6\right)-\frac{1}{4}F^2\right]+\oint_{z=\epsilon}\mathrm{d}^3x\sqrt{h}(-2K+2\gamma)\,, \tag{5.32}$$

where g_E is the Euclidean metric, h is the induced metric on a hypersurface normal to a radial (z) slice, pointing outwards, K is the trace of the extrinsic curvature and $\gamma = 2$ is required to make the AdS free energy vanish. The imaginary time at temperature T is compactified with the radius $\beta = 1/T$, the integral in the x–y plane produces the (infinite) volume Vol_2, and the radial integration is performed to some UV cutoff ϵ, yielding

$$S_E = \beta\mathrm{Vol}_2\int \mathrm{d}z\sqrt{g_E}\left[\frac{1}{2\kappa^2}\left(R+6\right)-\frac{1}{4}F^2\right]+\beta\mathrm{Vol}_2\sqrt{h(\epsilon)}(-2K(\epsilon)+2\gamma)\,. \tag{5.33}$$

This accounts for the contribution of the bosonic fields. The Dirac action vanishes on-shell and therefore does not contribute to this part. It does have a one-loop contribution to the free energy density

$$f \equiv \frac{S_E}{\beta\mathrm{Vol}_2}+f_{\mathrm{Dirac}}\,. \tag{5.34}$$

Here f_{Dirac} represents the fermionic contribution. Following [47, 226, 223, 227], at $T = 0$ we can simply sum the energies along the filled band of fermions (above the Dirac sea). This is the internal energy shifted by the chemical potential. For our normal modes, this leads to the expression

$$f_{\mathrm{Dirac}} = \sum_\ell \int \frac{k\mathrm{d}k}{2\pi}\,\Theta(-E_\ell(k))\Theta(E_\ell(k)-\mu q)E_\ell(k) = \int \frac{k\mathrm{d}k}{2\pi}\,\Theta(-E_1(k))E_1(k)$$

where in the last line we have made explicit that we choose our chemical potential such that only states of the lowest electronic radial mode $E_{\ell=1}$ will be occupied. One must first choose the potential strength λ such that the Schrödinger potential supports at least one normalizable mode. At the same time, it is only these normalizable modes that can be populated. If there is only one band in the window of existence of normalizable modes $[\omega_-(k),\omega_+(k)]$, *i.e.*, $E_{\ell=1}(k) < \omega_+(k) < E_{\ell=2}(k)$, then increasing the chemical potential beyond that upper limit will not populate further normalizable modes. Our rQES is in this sense not plagued by the usual large-N Fermi surfaces artifact.

It is furthermore quite easy to show that both before and after accounting for backreaction the band structure follows a similar form as in pure AdS_4 [47]

$$E_\ell(k) = -E_0+\sqrt{k^2+k_0^2}\,, \tag{5.35}$$

where $k_F \equiv \sqrt{E_0^2-k_0^2}$ and the parameters E_0, k_0 are most easily found by fitting from the numerical dispersion curves, as in Fig. 5.6.

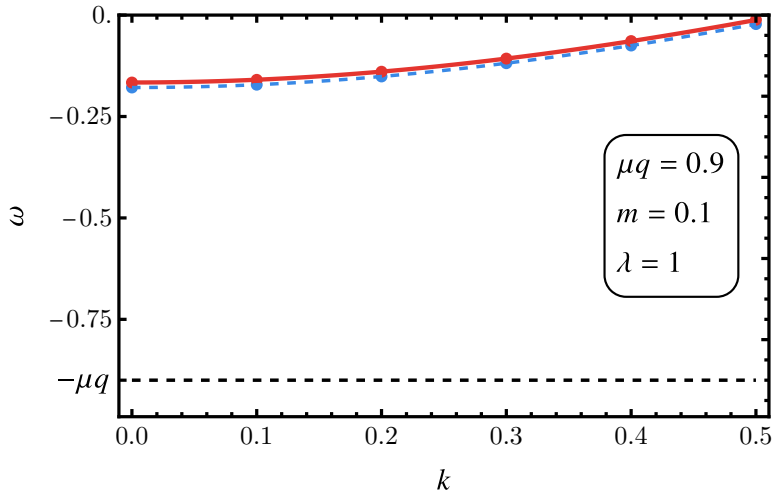

Figure 5.6: First electronic band for $\{m, \mu q, \lambda\} = \{0.1, 0.9, 1\}$, for the AdS_4 background with constant electrostatic potential (blue) and the backreacted solution (red). The lines are a fit to the form (5.35).

Note that f_{Dirac} is negative semi-definite. This does not mean, however, that the occupied state is automatically thermodynamically preferred. The backreaction also changes the bosonic saddle point contribution compared to its original AdS_4 value $f(AdS_4) = 0$. Adding both contributions we compare to the RN free energy

$$f(\text{RN}) = -\frac{4 + z_h^2 \mu^2}{4 z_h^3} = -\frac{\mu^3}{6\sqrt{3}} \text{ at } T = 0 \,. \tag{5.36}$$

Because the regulator does not act on the background sector, the Reissner-Nordström free energy is unaffected by it.

Fig. 5.7 shows the free energy of the rQES as a function of the charge μq for a fixed mass m and confining potential strength λ. As q increases, the rQES grows, so we need to compute more and more modes. This becomes more and more time consuming. By constructing an interpolating curve based on low q rQES solutions (using the points until $\mu q \simeq 1.2$), we can estimate where the solution becomes thermodynamically preferred and verify this with a fewer number of large q datapoints ($\mu q = 1.4$ and $\mu q = 1.58$). We see that at $\mu q = \mu q_c \simeq 1.56$, the rQES becomes thermodynamically preferable over the RN background.

In Fig. 5.8a, we show that this transition point evolves linearly with the fermion mass m for fixed q and λ. Based on this finding, we can sketch a thermodynamic phase diagram for our model in Fig. 5.8b. The critical charge satisfies an approximate relation $q_c(m;\lambda) \approx c_0(\lambda) + c_1(\lambda)\frac{m}{\mu}$ with c_0 and c_1 dependent on λ. It is tempting to compare this to the confounding phase diagram based on RN holography alone. For pure RN

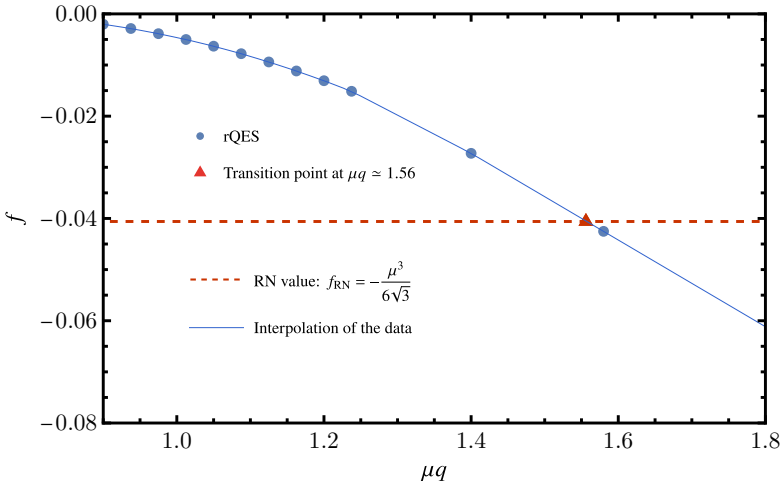

Figure 5.7: Plot of the free energy density for rQES at $\{\mu, m, \lambda\} = \{0.75, 0.1, 1\}$ as a function of the fermionic charge μq (blue dots) and the reference RN black hole free energy (red dashed line); the thin blue line and the red triangle are to guide the eye to the transition point. Since RN has no fermions its free energy curve is flat, *i.e.*, does not depend on the fermion charge. The first-order phase transition from RN to rQES happens at the intersection of the two lines. Since the calculations for larger μq values are costly, we only compute two points for $\mu q > 1.5$ and interpolate.

holography it is surmised [33] that the superradiant instability of the RN black hole toward an electron star (seen in the spectrum as log-periodic oscillations) sets in at $q = \sqrt{3}m$. This should correspond to the limit $\lambda \to 0$. As λ decreases we therefore expect the phase-boundary to pivot anti-clockwise. This comparison should be done with care, because the smaller λ becomes, the harder it is to observe bands that can be occupied — see the section on removing the regulator below. Another way to see this is that the effective Schrödinger potential in the extremal RN black hole for $\omega = k = 0$ (the onset of instability) has no linear term in m: $V_{\mathrm{RN}} \sim -4q^2 + 2m^2$. Hence we cannot extrapolate freely to $\lambda = 0$.

5.3.2 Spectrum of the rQES

To confirm our results, we consider the fermionic spectral function on rQES backgrounds. As a reminder, the spectral function is defined as the trace of the imaginary part of the retarded propagator: $A(\omega, k) = \mathrm{Im}\,\mathrm{Tr}\,G_R(\omega, k)$. In holography the type of propagator is defined by the boundary conditions in the interior. Therefore the only difference with computing the normalizable Dirac solutions is the choice of appropriate boundary conditions.

Considering that we have an emergent AdS_4 geometry in the IR, we can use the known prescription for infalling boundary conditions in pure AdS, *i.e.*, the presence of

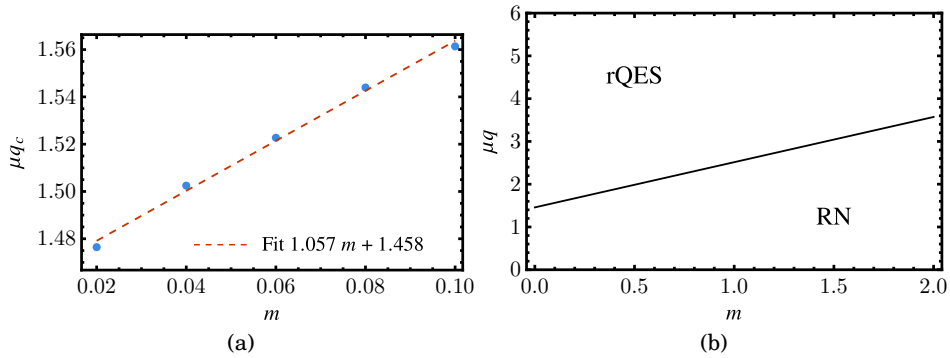

Figure 5.8: (a) Transition point μq_c as a function of m and its linear fit, for $\lambda = 1$. (b) Sketch of the phase diagram of the rQES. The black line indicates a first order transition between the regulated Reissner-Nordström and the rQES, occuring when their free energies cross.

a Poincaré horizon [228]. Accounting for the confining potential, these are

$$\psi_1(z \to \infty) = \begin{cases} e^{-z\sqrt{\boldsymbol{k}_{\rm IR}^2}}, & \text{if } \omega_{\rm IR}^2 < k_{\rm IR}^2 + \lambda_{\rm IR}^2 \,, \\ e^{iz\sqrt{-\boldsymbol{k}_{\rm IR}^2}}, & \text{if } \mathrm{Re}[\omega_{\rm IR}] > \sqrt{k_{\rm IR}^2 + \lambda_{\rm IR}^2} \,, \\ e^{-iz\sqrt{-\boldsymbol{k}_{\rm IR}^2}}, & \text{if } \mathrm{Re}[\omega_{\rm IR}] < -\sqrt{k_{\rm IR}^2 + \lambda_{\rm IR}^2} \,, \end{cases} \tag{5.37}$$

where $\omega_{\rm IR}, k_{\rm IR}, \lambda_{\rm IR}$ were defined by (5.25), $\boldsymbol{k}_{\rm IR} = (\omega_{\rm IR}, \sqrt{k_{\rm IR}^2 + \lambda_{\rm IR}^2}, 0)$ and $\boldsymbol{k}_{\rm IR}^2 = -\omega_{\rm IR}^2 + k_{\rm IR}^2 + \lambda_{\rm IR}^2 = V_{\rm IR}$. As we saw with the normal modes, the IR boundary condition for ψ_2 can be obtained using the Dirac equation and the boundary condition for ψ_1. After imposing these boundary conditions, the retarded propagator is then computed as

$$G_R(\omega, k) = B/A = \lim_{z\to 0} z^{-2m} \frac{\psi_1(z)}{\psi_2(z)} \,, \tag{5.38}$$

where A and B are the coefficients in the UV expansion of the spinor (5.20).

Inside the gap ($\omega_{\rm IR}^2 < k_{\rm IR}^2 + \lambda_{\rm IR}^2$) the IR boundary conditions are the same for the probe fermions as for the bulk normalizable modes – the wavefunction should fall off for $z \to \infty$, which yields $A = 0$ for the normal mode frequencies $\omega = E_\ell(k)$. Therefore, the propagator will present a pole along the bands of the background. Moreover, since the fermionic wavefunctions and thus also the Green's functions are real inside the domain where bound states exist, the spectral function will vanish there. Thus, we expect to see $\mathrm{Im}\, G_R(\omega, k) = 0$ for $\omega \in \left[\omega_-(k), \omega_+(k)\right]$, except when $\omega = E_\ell(k)$ where a pole should appear.

This general structure of the spectral function including the gap for $\omega_- \le \omega \le \omega_+$ can be seen in Fig. 5.9. The data here and in the remainder of this section is computed

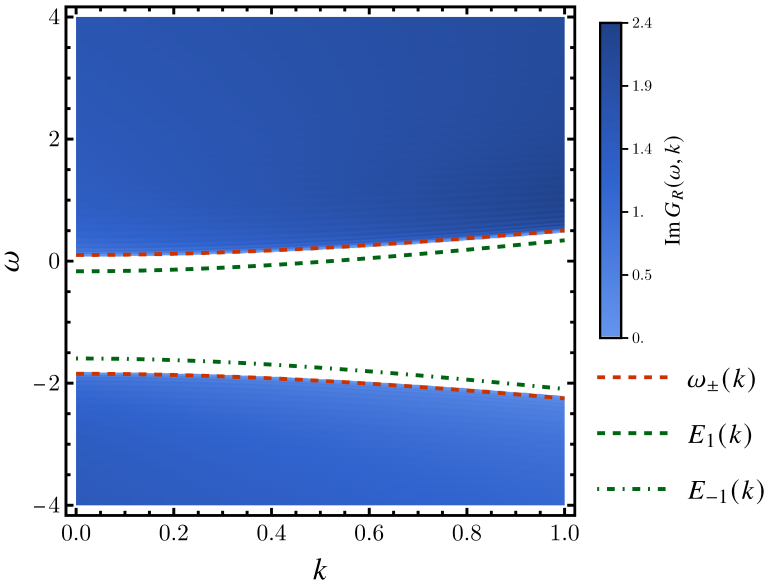

Figure 5.9: Spectral function $\mathrm{Im}G_R(\omega,k)$ for $\{m,\mu q,\lambda\}=\{0.1,0.9,1\}$. The gap appears in white and is well delimited by $\omega_\pm(k)$ (red dashed lines). The normal mode bands have been superimposed to show the infinitely long-lived modes, see Fig. 5.10. Outside the gap, there is no particle (normal mode) but a continuum shaped by the remnant of the UV conformal branch cuts. Since the regulator and the chemical potential explicitly break conformality, we do not reproduce the pure AdS Lorentz-invariant spectrum for any finite value of ω and k.

for $\{\mu,q,m,\lambda\}=\{3/4,1.2,1/10,1\}$. Inside the gap (white area), the spectral weight of excitations is indeed zero to numerical accuracy except at the positions of the normal modes of the background fermions. The latter are computed directly from the solution of the background Dirac equation (green lines in Fig. 5.9), as they cannot be seen numerically in the spectral function because they are infinitely long-living modes which show in the spectrum as Dirac delta peaks. Being infinitely narrow on the real axis, they can only be detected in the complex-ω plane. Representing schematically the normal mode located at $\omega_\star$ by $\mathrm{Im}G(\omega=\mathrm{Re}(\omega))=Z\delta(\omega-\omega_\star)$ where Z is the peak weight (wavefunction renormalization), we have, for complex ω:

$$\mathrm{Im}G_R(\omega,k)=-Z\frac{\mathrm{Im}\,\omega-\mathrm{Im}\,\omega_\star}{\left(\mathrm{Re}\,\omega-\mathrm{Re}\,\omega_\star\right)^2+\left(\mathrm{Im}\,\omega-\mathrm{Im}\,\omega_\star\right)^2}\,. \tag{5.39}$$

When $\mathrm{Re}\,\omega=\mathrm{Re}\,\omega_\star$, this simplifies to

$$\mathrm{Im}G_R(\omega,k)=-\frac{Z}{\mathrm{Im}\,\omega-\mathrm{Im}\,\omega_\star}\,. \tag{5.40}$$

We check this picture against the numerics first in Fig. 5.10 (A), where the absolute value of the spectral function in complex frequency plane shows the typical structure

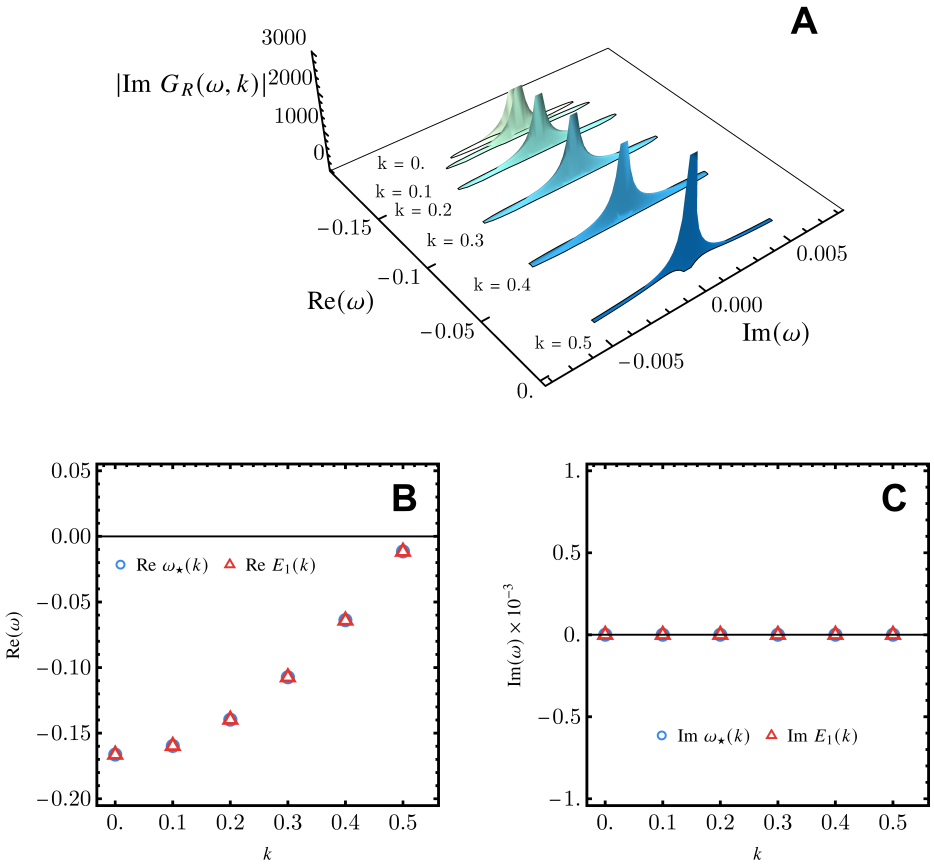

Figure 5.10: (A) Absolute value of the fermionic spectral function for different values of momentum. The plot is cropped for values below 100 to highlight the quasiparticle peaks. (B and C) Comparison of the poles in the spectrum (blue circles), identified in (A), to the first electron band of the background (red triangles). The real parts (B) of both sets agree perfectly; the imaginary parts (C) are both zero to high accuracy. All this data is computed for $\{m, \mu q, \lambda\} = \{0.1, 0.9, 1\}$.

of a string of poles (for various momentum values) lying on the real axis. The relation (5.40) is then used to identify the dispersion relation of the pole $\omega_\star(k)$ by fitting $\mathrm{Im}G_R(\omega,k)$. We find, with no big surprise, a perfect agreement with the normal mode excitations $E_1(k)$ corresponding to the first electron band, as seen in Fig. 5.10 (C) and (D). A similar picture is found for the first hole band $E_{-1}(k)$ and this yields the spectrum inside the gap, plotted in Fig. 5.9.

In Fig. 5.11 we compare the spectral function at finite μ for our regulated quantum electron star (blue data points) to the fermionic spectral function in a pure AdS_4 background with finite chemical potential, either with (green line) and without (red line) regulation by the confining scalar. The comparison is given at $k = 0$ (left) and $k = 1$ (right). The Dirac spectrum in AdS_4 is well-known [228]:

$$G_R(\omega,k) = \begin{cases} \dfrac{2}{\omega^2-k^2}\dfrac{\Gamma(1/2-m)}{\Gamma(1/2+m)}\left[-\dfrac{i}{2}\left(\omega^2-k^2\right)\right]^{2m+1}\left[\omega\gamma^0-k\gamma^1\right] & \text{if } \omega > k\ , \\ \dfrac{2}{\omega^2-k^2}\dfrac{\Gamma(1/2-m)}{\Gamma(1/2+m)}\left[\dfrac{i}{2}\left(\omega^2-k^2\right)\right]^{2m+1}\left[\omega\gamma^0-k\gamma^1\right] & \text{if } \omega < -k\ . \end{cases} \tag{5.41}$$

It has a conformal branch-cut at $\omega = k$ and a gap for $\omega^2 < k^2$. For AdS_4 with finite electrostatic potential, one merely needs to replace $\omega \to \omega + \mu q$ in the previous expression. Adding confining potential by turning on the chirality-breaking flat scalar widens the gap to $(\omega+\mu q)^2 < k^2 + \lambda^2$; in particular the gap is open also at $k = 0$. The rQES solution outside the gap exhibits qualitatively the same spectral function as that of the confined Dirac spectrum in pure AdS_4 but for renormalized IR values $\omega_{\mathrm{IR}}, k_{\mathrm{IR}}, \lambda_{\mathrm{IR}}$ given in (5.25). It is important to emphasize that none of the modes in this continuum are normalizable and thus do not contribute when building the bulk rQES, even when μq is large enough that $\omega_+(k) < 0$. This is guaranteed by our choice of UV boundary conditions.

5.4 Towards a self-confining quantum electron star

5.4.1 Comparison to the holographic superconductor

By construction the confinement in our setup gives an AdS_4-to-AdS_4 solution. With the fully backreacted solution in hand we can also understand what the field theory dual describes. The confining regulator scale λ gaps the field theory fermion spectral function. Considering then the RG flow from the IR emergent conformal field theory towards the UV, this means that as one increases the energy scale it takes a finite distance for occupiable fermion states to be encountered. This can also be seen in the band structure of Fig. 5.6. At this scale the theory deforms away from the strict conformal theory up to the scale μ beyond which it is no longer energetically favorable to occupy more states. The flow up the RG then continues towards the UV AdS_4 fixed point.

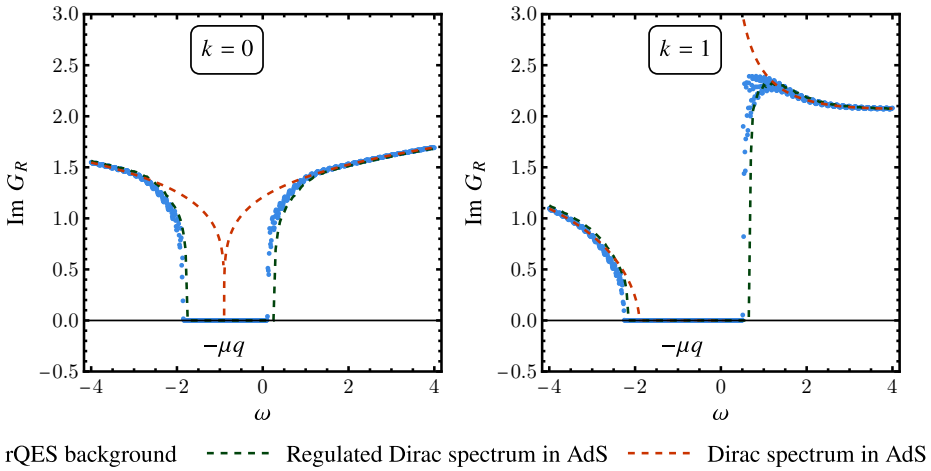

Figure 5.11: (Confined) Dirac spectral function (blue points) in the rQES background for $k = 0$ (left) and $k = 1$ (right), compared with the standard/unconfined (red dashed line) and regulated/confined (green dashed line) Dirac spectral function in AdS with finite electrostatic potential.

In the more usual flow from the UV to the IR this is not a natural RG trajectory. The generic IR will not be a non-trivial conformal field theory. Nevertheless, within holography such AdS_4-to-AdS_4 domain walls are well-known. Especially in the search for the holographic dual of the holographic superconductor ground state, Horowitz and Roberts and independently Gubser and Rocha have found AdS_4-to-AdS_4 domain walls (in some cases with logarithmic corrections) in a finite parameter range [217, 218]; the other solution found is the Lifshitz geometry. It was later understood that Lifshitz rather than an AdS_4 IR is the generic holographic superconductor ground state [218, 41], but this is only seen with the inclusion of a stabilizing quartic potential.

In detail of course the solutions are different. The Horowitz-Roberts-Gubser-Rocha holographic superconductor ground states do not need an additional confining scalar. They can also be obtained classically without the need for a one-loop Hartree mean field. This is due to the fact that the bosonic field already couples quadratically to the electrostatic potential A_t. A fermion only couples linearly, but its one-loop contribution can couple at all orders. This is why for fermionic systems one needs to go to one-loop.

5.4.2 Confinement in the rQES solution

Given that the Horowitz-Roberts-Gubser-Rocha AdS_4-to-AdS_4 solutions do not need a confining potential, and that the more generic holographic superconductor Lifshitz solutions are known, it is a natural question why we do not try to remove the soft-confining regulator altogether. There was in fact a concerted effort to do so several years ago [42, 48, 46], culminating in the QES model of [49, 50]. The latter two articles

show in detail how the presence of the gap and the discretized spectrum are crucial to construct any type of quantum fermionic backreacted solution, *i.e.*, where one or a small finite number of radial modes are occupied. Any attempt to remove the confining potential results in a uncontrolled continuum spectrum.

It is precisely this insight that was the starting point for our confining potential. What we have furthermore shown, is that even then there are several severe technical hurdles to overcome to construct a converging fully backreacted confined quantum electron star solution. At the same time the general insight still holds. Our infrared boundary conditions crucially depend on the coupling to the scalar $\Phi(z)$ to extend the domain of existence of normalizable modes of AdS_4 all the way to $k = 0$. The parameter λ, as we previously noted, acts as a momentum shift in this domain such that a mode at $k = 0$ will behave as a mode at $k_{\text{eff}} = \lambda$ and therefore normalizable modes with $|\omega + \mu q| < \lambda$ will be found. These can be populated and will condense in the bulk. Turning off the potential, even slowly, will invariably lead to a lack of normalizable modes at the lowest momenta and will bring us back to a situation similar to that of AdS_4.

One sliver of hope would be that the domain wall solution itself, after convergence, can support a well in the Schrödinger potential such that a regulator is no longer necessary. We have therefore looked at this (Fig. 5.12) by comparing the Schrödinger potential for a $k = 0$, $\omega = E_1(0)$ mode in the confined quantum electron star AdS_4-to-AdS_4 background with and without the confining potential. Without a potential, however, the AdS_4-to-AdS_4 quantum electron star domain wall solution is not confining. We do see that $V_{\text{domain wall}}(z \to \infty) > V_{\text{AdS}}$ which means the wedge of existence of normalizable modes is indeed wider in the domain wall solution than in the AdS_4 solution. Yet, the modes with sufficiently small momenta (including $k = 0$) are always outside the wedge.

This therefore leads us to believe a true QES would not *remove* the regulator but must *incorporate* it into the model, *i.e.*, make the scalar field a dynamical dilaton which couples to the Dirac fermion and drives the geometry from one fixed point to another.

5.5 Discussion and conclusions

In this paper we have constructed a self-consistent model of a single band confined holographic Fermi liquid. The crucial technical problem, the infrared divergence brought about by the fermionic wavefunctions, is solved by controlling it by hand. We control the far infrared by the means of a scalar regulator, equivalent to a soft-confining potential. The confinement is drastic and 100%: our regulated quantum electron star is dual to a gas of infinitely-long living particles with zero self-energy. In the limit where we compute, it is a single-band Fermi-gas rather than a Fermi-liquid.[6] At higher

[6]This holds at zero temperature. At finite temperature a black hole horizon would form, causing inevitably some dissipation even in the presence of the confinement.

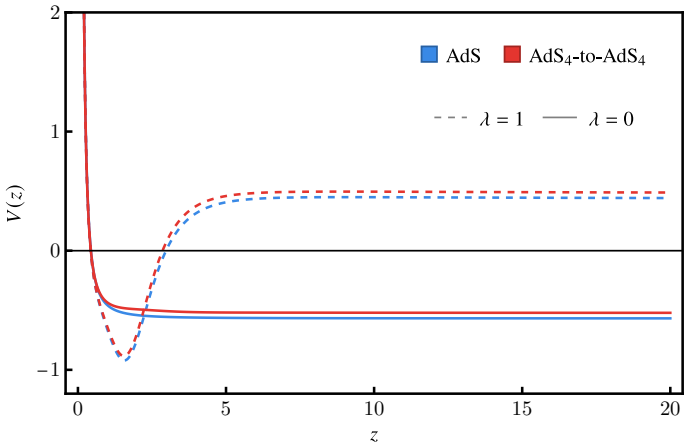

Figure 5.12: Comparison of the Schrödinger potential for the AdS_4 (blue) and AdS_4-to-AdS_4 (red) solutions with (dashed) and without (solid) regulator, for $\{m, \mu q, k, \omega\} = \{0.1, 1.05, 0, -0.027\}$.

energies, the spectrum switches to the featureless continuum inherited from the UV conformal field theory (though it is not conformally invariant due to the presence of the confining potential).

The regulated quantum electron star is the thermodynamically preferred solution over the Reissner-Nordström background for $\mu q/m > (\mu q/m)_{\text{critical}}$. The transition is first order, which means that the there is no continuous exchange of charge from the RN solution to the bulk Fermi sea. Instead all the charge is carried by the infinitesimally small rQES. This is somewhat different from the conundrum that we mention in the Introduction: the onset of a log-oscillatory signal in the spectral function signaling a putative instability and the presence of normalizable solutions. The first order transition is essentially unrelated to the RN horizon instability.

Although it is not yet clear how the rQES is related to the final state after the conjectured continuous quantum phase transition which destroys the Reissner-Nordström black hole horizon signalled by the log-oscillatory instability, we nevertheless feel it is a step in the right direction, bringing us closer to the full unregulated quantum electron star. The reasons are the following:

1. It is now much clearer what a healthy Fermi liquid should do on the gravity side: it should self-consistently form a geometry which yields such an effective potential for the Dirac fermion that it is just confined enough not to diverge in far IR but not so much that the bulk Fermi sea dies out in the far IR, failing to influence the low-energy physics.

2. We have inspected in some detail the spectrum and the phenomenology of the dual confined Fermi liquid. Although our confining bulk construction is somewhat more natural in holography – it just uses a non-dynamical rather than

a dynamical scalar — than the hard-wall model [47], and it now allows us to compute the backreaction, qualitatively the field-theory side description is only marginally improved. Similar to the hard-wall model, the occupied fermions have vanishing self-energy. The main effect of the backreaction is to understand how this confined Fermi gas emerges in an RG flow from the UV conformal field theory. In the likely event that an unregulated (confining) quantum electron star — supported for instance by a dynamical rather than a non-dynamical scalar (such as the fluid electron star in [45]) — has a Lifshitz IR rather than an AdS_4 IR, possible decay into the Lifshitz horizon could provide a finite lifetime and an honest Fermi liquid.

3. Unlike the global AdS radius regulator of [50] which cannot be easily be sent to infinity, our scalar can at least in principle be made dynamical. That would be a perfectly natural holographic model, given the ubiquity of non-minimally coupled scalars in top-down holographic actions. Therefore, a very natural line of further research is to turn this construction into a fully dynamical Einstein-Maxwell-Dirac-scalar system, similar to the fluid approach of [45].

Apart from the natural next step – making the dilaton dynamic – a number of other directions of work open up. It would be useful to understand the relation of our work to the AdS/QCD studies, some of which employ a similar type of scalar (soft wall) to impose confinement. The role of the Fock correction (the one-loop exchange diagram) is also not clear yet, and may be important for a fully self-regulating solution and/or a finite self-energy. Finally, the most characteristic property of rQES – the domain-wall-type solution with an infrared AdS_4, is analogous to the domain-wall holographic superconductor solutions of Horowitz-Roberts-Gubser-Rocha [41, 217, 229]. Based on those results and the macroscopic electron star with dynamical dilaton studied in [45], it strongly suggests that Lifshitz IR quantum electron stars must also exist.

Acknowledgements

We thank Jan Zaanen for discussions. This research was supported in part by the Netherlands Organization for Scientific Research (NWO), the Netherlands Organization for Scientific Research/Ministry of Science and Education (NWO/OCW), Ministry of Education, Science and Technological Development of the Republic of Serbia and Science Fund of the Republic of Serbia, under the Key2SM project (PROMIS program, Grant No. 6066160).